Localization of the source of quasiperiodic VLF emissions in the magnetosphere by using simultaneous ground and space observations: a case study

A. G Demekhov.[1,2], E. E. Titova[1,3], J. Manninen[4], D. L. Pasmanik[2], A. A. Lubchich[1], O. Santolík[5,6], A. V. Larchenko[1], A. S. Nikitenko[1], and T. Turunen[4]

[1]Polar Geophysical Institute, Apatity, Russia
[2]Institute of Applied Physics, RAS, Nizhny Novgorod, Russia
[3]Space Research Institute, RAS, Moscow, Russia
[4]Sodankylä Geophysical Observatory, Sodankylä, Finland
[5]Department of Space Physics, Inst. Atmospher. Phys., Czech Acad. Sci., Prague, Czechia
[6]Faculty of Mathematics and Physics, Charles University in Prague, Czechia

Key Points:

- Complex analysis of generation region of quasi-periodic VLF emissions observed simultaneously by two Van Allen Probes and on the ground
- Wave growth rate frequency band matched the observed emission band in a localized region along Van Allen Probe A trajectory
- Ray tracing demonstrated the importance of a density duct for wave exit to the ground

Corresponding author: Andrei Demekhov, andrei@ipfran.ru

Abstract

We study quasi-periodic VLF emissions observed simultaneously by Van Allen Probes spacecraft and Kannuslehto and Lovozero ground-based stations on 25 December 2015. Both Van Allen Probes A and B detected quasi-periodic emissions, probably originated from a common source, and observed on the ground. In order to locate possible regions of wave generation, we analyze wave normal angles with respect to the geomagnetic field, Poynting flux direction, and cyclotron instability growth rate calculated by using the measured phase space density of energetic electrons. We demonstrate that even parallel wave propagation and proper (downward) Poynting flux direction are not sufficient for claiming observations to be in the source region. Agreement between the growth rate and emission bands was obtained for a restricted part of Van Allen Probe A trajectory corresponding to localized enhancement of plasma density with scale of 700 km. We employ spacecraft density data to build a model plasma profile and to calculate ray trajectories from the point of wave detection in space to the ionosphere, and examine the possibility of their exit to the ground. For the considered event, the wave could exit to the ground in the geomagnetic flux tube with enhanced plasma density, that ensured ducted propagation. The region of wave exit was confirmed by the analysis of wave propagation direction at the ground detection point.

1 Introduction

There are many different types of natural electromagnetic VLF emissions, such as hiss, chorus, and quasiperiodic emissions observed both on the ground and by spacecraft for more than 50 years. A rich collection of early observations was presented by Helliwell (1965). It is generally accepted that these types of VLF emissions are generated due to electron cyclotron interaction with energetic electrons (Trakhtengerts, 1963; Kennel & Petschek, 1966).

Recently, characteristics of the sources of different types of VLF emission generated during the development of the cyclotron instability in the magnetosphere have been actively discussed. For this purpose, multispacecraft measurements of VLF waves are often used. For example, Santolík and Gurnett (2003) analyzed individual elements of VLF chorus on four Cluster satellites at $L = 4.4$, determined the typical coherence scale of the chorus amplitude of about 100 km across the geomagnetic field which is of the order of the wavelength. Using coordinated observations of Van Allen Probe and THEMIS,

Li et al. (2015) confirmed the idea that chorus waves generated at high L shell (~ 10) can be a source of plasmaspheric hiss (Chum & Santolík, 2003; Santolík et al., 2006; Bortnik et al., 2009).

Simultaneous ground and satellite observations of the same VLF emissions were also used for localizing their source. However, such observations are still quite rare. Most of them deal with quasiperiodic (QP) emissions that are characterized by periodic or quasiperiodic modulation of wave intensity with periods from several seconds to minutes. Their main properties are described in a review by Sazhin and Hayakawa (1994). Similarity of the frequency-time spectra of quasiperiodic (QP) emissions detected simultaneously by the low-orbiting DEMETER satellite ($h \approx 700$ km) and on the ground was reported by Němec et al. (2016). During those events, the spacecraft crossed a wide range of invariant latitudes, which, to our mind, might indicate the nonducted propagation of the VLF signals. However, the variation of the intensity with the spacecraft latitude indicates, according to Němec et al. (2016) that the sources of QP emissions detected on the ground were near the plasmapause and the waves propagated along it in the waveguide regime described by Inan and Bell (1977) and Semenova and Trakhtengerts (1980). Němec et al. (2018) showed that the majority of QP observations onboard Van Allen Probes (Radiation Belt Storm Probes, hereafter RBSP) took place in the plasmasphere.

Recently, QP emissions detected both on the ground and by Van Allen Probes spacecraft in the equatorial region were compared (Titova et al., 2015; Martinez-Calderon et al., 2016). One-to-one correspondence between the quasiperiodic elements detected on the ground and by Van Allen Probe-A (RBSP-A) was found in a wide range of L shells from 3.0 to 4.3 (Titova et al., 2015), which was explained by nonducted propagation of QP emissions. By comparing the wave properties and the evolution of electron distribution function during the event, Titova et al. (2015) identified the possible location of QP emissions source at about $L = 4$, and its radial extent was $\Delta L \approx 0.3$, i.e., much smaller than the region of wave observation. This conclusion was further confirmed by calculations of the wave growth rate on the basis of the measured energetic-electron distribution (Lyubchich et al., 2017). Martinez-Calderon et al. (2019) analyzed ERG observations, and their results also indicate that the QP emissions can be detected outside of the generation flux tube.

QP emissions detected at subauroral latitudes on the ground and by RBSP-A in the equatorial region were compared by Martinez-Calderon et al. (2016). The similarity of dynamic spectra of QP elements was demonstrated and the time delay of conjugate QP elements was determined for one element. Based on spacecraft measurements of the plasma density, the authors calculated the trajectories of nonducted VLF waves and thus explained the observed delay between the QP elements detected by the satellite and the ground-based station. Therefore Martinez-Calderon et al. (2016) concluded that the quasi-periodic emissions detected at a subauroral ground station propagated in the nonducted mode in the magnetosphere. Němec et al. (2013) also demonstrated that QP emissions observed by the Cluster spacecraft often propagate from the equator in a nonducted mode, i.e., obliquely with respect to the magnetic field lines. It is clear that nonducted propagation significantly complicates the localization of the source region of QP emissions. On the other hand, Manninen et al. (2014) analyzed the periodic fine structure of QP elements observed by the ground based subauroral station Kannuslehto (KAN) in Northern Finland, and revealed its correspondence to the time scales of guided field-aligned propagation of whistler-mode waves. Based on this fact they concluded that the QP emissions observed at KAN propagated in the ducted regime. Demekhov et al. (2017) and Titova et al. (2017) analyzed simultaneous observations of VLF emissions at KAN and by RBSP for the event of December 25, 2015, when chorus, QP emissions, and unstructured hiss were recorded. Those authors have shown that the exit of VLF signals, including QP emissions, to the ground was possible due to the wave guiding in the observed ducts with enhanced density.

Němec et al. (2018) have shown that the majority of QP emissions observed by Van Allen Probes in the equatorial region had low wave normal angles ($< 20^\circ$). However, that conclusion was made by using only waves with sufficiently high planarity ($p > 0.5$), which constitute about 1/4 of all events. Overall, the question how the QP emissions propagate in the magnetosphere and exit to ground has not yet been answered.

In this paper, we try to localize the possible generation region of the QP emissions and study the mechanism of their exit to the ground for a specific QP event with a period of about 20-30 s detected simultaneously at KAN, Lovozero station (LOZ), and by Van Allen Probes on 25 December 2015. The used data are described in Section 2, and the observations are presented in Section 3. As the preliminary criteria of the possible source location, we use quasi-parallel propagation of the whistler mode waves detected

by Van Allen Probes and their Poynting flux direction from the geomagnetic equator. However, a more careful analysis turns out to be necessary. In Section 4.1 we calculate the growth rate of whistler mode waves by using the spacecraft measurements of energetic particles and compare it with the spectrum and intensity of the observed VLF waves. Agreement between the growth rate and VLF wave spectra together with off-equatorial Poynting flux direction and quasi-parallel wave propagation is considered as a more reliable indicator of possible source location. In Section 4.2, we consider the VLF wave propagation by using ray tracing calculations and analyze conditions for the wave exit to the ground. Section 5 presents our conclusions.

2 Data

The twin Van Allen Probes spacecraft were launched on 30 August 2012 into near-equatorial elliptical orbits with $\approx$ 700 km perigee and $\approx 5.8R_E$ apogee. Both RBSP-A and RBSP-B spacecraft have the same orbit, but RBSP-A has a delay of about 1 h. In this paper, we use VLF wave and plasma density measurements from both spacecraft.

The wave measurements were made by the Electric and Magnetic Field Instrument Suite and Integrated Science (EMFISIS) that provides data on DC magnetic fields and three components of electric and magnetic fields (Kletzing et al., 2013). We used the data from the survey mode available from the EMFISIS wave instrument. In this mode, the EMFISIS/WAVES instrument measures the wave power spectral densities, relative phases, and coherencies of electric and magnetic field components from 2 Hz up to 12 kHz in 0.5-s intervals every 6 s. This data set allowed us to obtain power spectral density and perform multicomponent wave analysis of ELF/VLF events (Santolík et al., 2014), as a result of which one can obtain the polarization of waves (Santolik & Gurnett, 2002), the wave-normal angles with the singular-value decomposition (SVD) method of (Santolík et al., 2003), and the Poynting vector using the spectral matrix method of (Santolík et al., 2010). The in situ cold plasma density was taken from the data on floating spacecraft potential provided by the Electric Fields and Waves (EFW) instrument (Wygant et al., 2013) for RBSP-B. We verified that they agreed well with EMFISIS data based on upper hybrid resonance emission (Kurth et al., 2015).

Fluxes of particles with energies of a few eV to tens of keV are recorded by HOPE (Helium, Oxygen, Proton, and Electron Mass Spectrometer) (Funsten et al., 2013). The

fluxes of electrons and protons (as well as helium and oxygen ions) are measured at 11 pitch-angles from 4.5° to 175.5° and in 72 energy channels with a time resolution of ∼ 20 s. The energy range is from 15 eV to 50 keV for electrons . The fluxes of particles with energies of tens of keV to a few MeV with a time resolution of ∼ 10 s are measured by the MagEIS (The Magnetic Electron Ion Spectrometer) (Blake et al., 2013). These fluxes are measured in 23 energy channels from 36 keV to ∼ 4 MeV at 11 pitch-angles in the range from 8° to 172°.

Ground-based observations of VLF signals were carried out in Northern Finland at KAN (67.74°N, 26.27°E; $L = 5.45$) and LOZ (67.98°N, 35.08°E; $L = 4.96$). VLF emissions at KAN were recorded in the frequency band from 0.2 to 39 kHz by using two mutually orthogonal magnetic loop antennas oriented in the geographical north-south and east-west directions. This allows one to calculate polarization characteristics of the signal and, in particular, to determine the azumuthal orientation of the polarization ellipse. The small axis direction gives approximate azimuth of VLF wave propagation with an ambiguity of 180°. Hereafter we term it the angle of arrival. The loops size is 10× 10 m with an effective area of 1000 m^2. The receiver sensitivity is about 0.1 fT, (i.e. ≈ 10^{-14} nT^2 Hz^{-1}). More detailed description of the hardware is given in Manninen (2005). The wide dynamic range of the receiver (up to 120 dB) allows us to detect both very weak and intense signals. The receiver at LOZ uses a similar magnetic antenna setup with 15× 16 m loops having 14 turns. In addition, there is a vertical electric field sensor that can be used to remove the 180° ambiguity of propagation direction. Details of the LOZ hardware can be found in Fedorenko et al. (2014).

3 Observations

The event occurred on 25 December 2015 from 11:00 to 13:00 UT. During this time interval, the QP VLF emissions were observed at KAN addand LOZ in frequency band $f = 3$–6 kHz with periods of 20–30 s. Geomagnetic activity was fairly low with the Dst index −4 nT, $Kp = 2$ and $AE \approx 100$ nT. Figure 1 shows, in geographic coordinates, the relative position of KAN and LOZ and the field-aligned projections of the RBSP-A and RBSP-B satellites to the ground in the northern hemisphere. The parts of spacecraft trajectories at which QP emissions had one-to-one correspondence to those detected at KAN are indicated by bold line segments. During the event both satellites were at lower geographic latitudes relative to KAN and moved inward. RBSP-B moved from $L =$

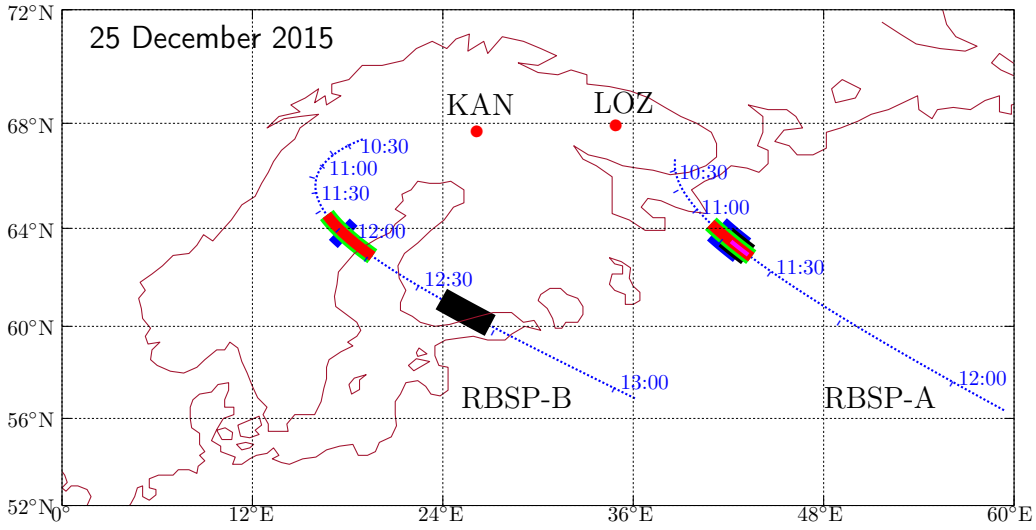

Figure 1. A map showing the location of KAN and LOZ ground stations (points) and the footprints of Van Allen Probes (thin lines) for the event on 25 December 2015. Thick blue segments mark the orbit parts where one-to-one correspondence of VLF emissions at the spacecraft and on the ground was observed. Green, red, and magenta segments indicate the time intervals corresponding, respectively, to low wave-normal angles (Figures 2d and 3d), Poynting vector direction from the equator (Figures 2e and 3e), and matching between the calculated growth rate and observed wave bands (Figure 6b). Black segments indicate crossing of the localized density enhancement (Figures 2e and 3e).

5.4 to $L = 2.9$ in the daytime sector from 13.1 to 15.6 MLT (magnetic local time) at the geomagnetic latitude (MLAT) from $-5°$ to $-15°$ (negative MLAT corresponds to the southern hemisphere). RBSP-A moved from $L = 4.6$ to $L = 2.9$ from 11:00 to 12:00 UT, being in the afternoon sector (14.4 to 16.1 MLT) at MLAT from $-11.6°$ to $-16.4°$.

3.1 VLF emissions observed by KAN and LOZ

Overview spectrograms of VLF signals detected by KAN are shown in Figures 2a (magnetic field spectral power) and 2b (angle of the minor axis of the polarization ellipse, i.e., angle of arrival relative to the geographic North). In Figure 3a, the spectrogram is repeated for comparison with RBSP-A. The emissions were observed in two fre-

quency bands $f = 3$–6 kHz and $f = 8.5$–10 kHz. In this paper, we discuss only the lower band, since QP emissions were observed there. In the higher frequency band $f =$ 8.5–10 kHz, individual bursts of narrow-band noise ($\Delta f < 1$ kHz) were detected with an increasing carrier frequency and duration of about 2 min; they were discussed by Titova et al. (2017).

Power spectra at LOZ are similar to KAN, so we show only the inverse angle of Poynting vector direction α_S (Figure 3b), since it allows us to resolve 180° ambiguity in the direction finding due to the additional measurement of vertial electric field.

QP emissions started at KAN and LOZ before the considered interval (about 10:20 UT) and continued with varying intensity and even breaks till 12:30 UT. The quasi-period varied within $\sim$ (20–30) s. In some parts of the event they were accompanied with noise (see, e.g., the interval 11:10 to 11:30 UT). We restrict the plotting interval for better visibility. No ground-spacecraft correlation was observed before 11:00 UT. Expanded views of quasi-periodic elements are given in Figures 4a and 5a. These spectra correspond to the intervals of correlation with RBSP-A and RBSP-B, respectively. The broadband signal detected by KAN at about 12:01:30 UT (Figure 5a) is the interference due to a car that was passing near the antennas.

It is seen in Figure 5a that the QP elements detected on the ground have a fine structure and consist of discrete elements with increasing frequency and the repetition rate of 4 s. This modulation corresponds to periodic emissions within QP emissions reported by Engebretson et al. (2004) and Manninen et al. (2014). Similar structure was observed during the interval shown in Figure 4a but it is less clearly visible. Sometimes there were chorus elements in the upper part of the QP emissions at frequencies around 5 to 7 kHz that were also observed by RBSP (Demekhov et al., 2017).

The angle between the minor axis of polarization ellipse and the direction to geographic North or South is shown in Figure 2b. It remains within the range of 50°–70° during the entire event and indicates that the waves arrived at KAN either from northwest or south-east. Taking into account that whistler-mode waves are generated below the equatorial electron gyrofrequency, and $f_{c\,\mathrm{eq}} \approx 5.3$ kHz at the L shell of KAN, the latter case seems more physically justified. This is consistent with the LOZ data presented in Figure 3b.

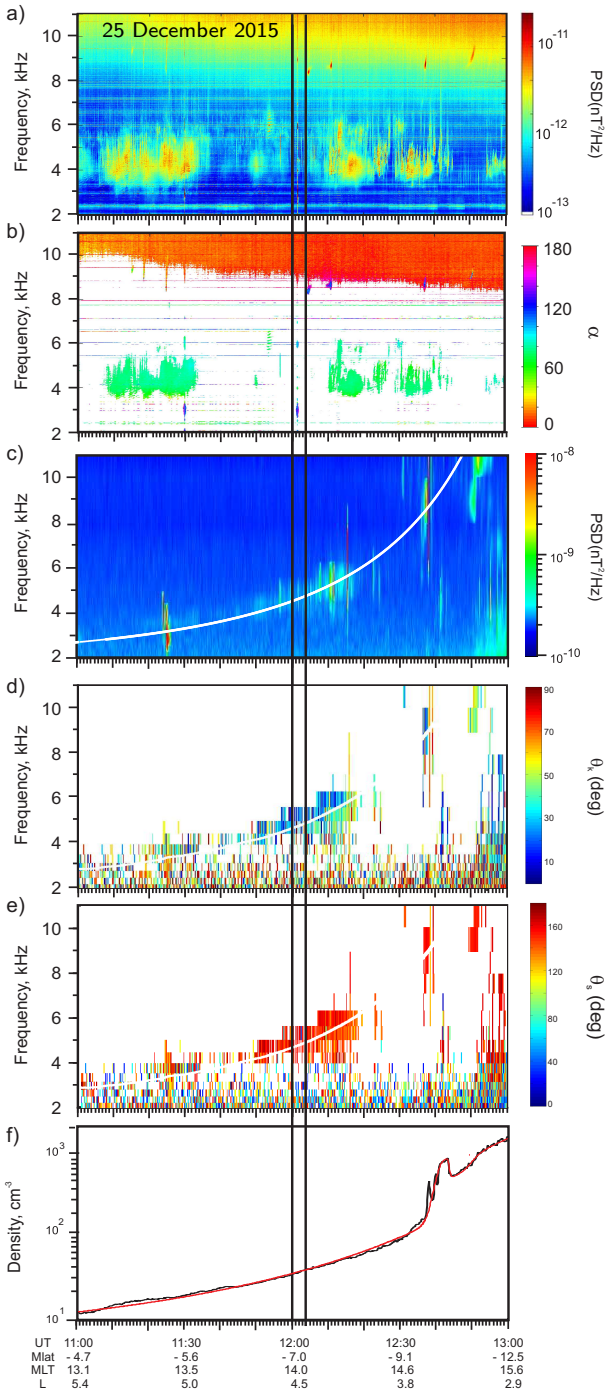

Figure 2. Frequency-time spectrograms of VLF emissions measured at KAN (a and b) and by the RBSP-B (c to e) on 25 December 2015 from 11:00 UT to 13:00 UT. (a) and (c) Magnetic power spectral density; (b) angle of arrival; (d) polar wave normal angle in the field-aligned coordinate system; (e) polar angle of Poynting flux. White curves show one half of the equatorial electron gyrofrequency ($f_{c\,\mathrm{eq}}/2$). Time interval corresponding to simultaneous observations of similar signals by KAN and RBSP-B is bounded by vertical lines. (f) Electron density derived from EFW data (black) and its smooth fit (red) that is used for ray tracing (Section 4.2).

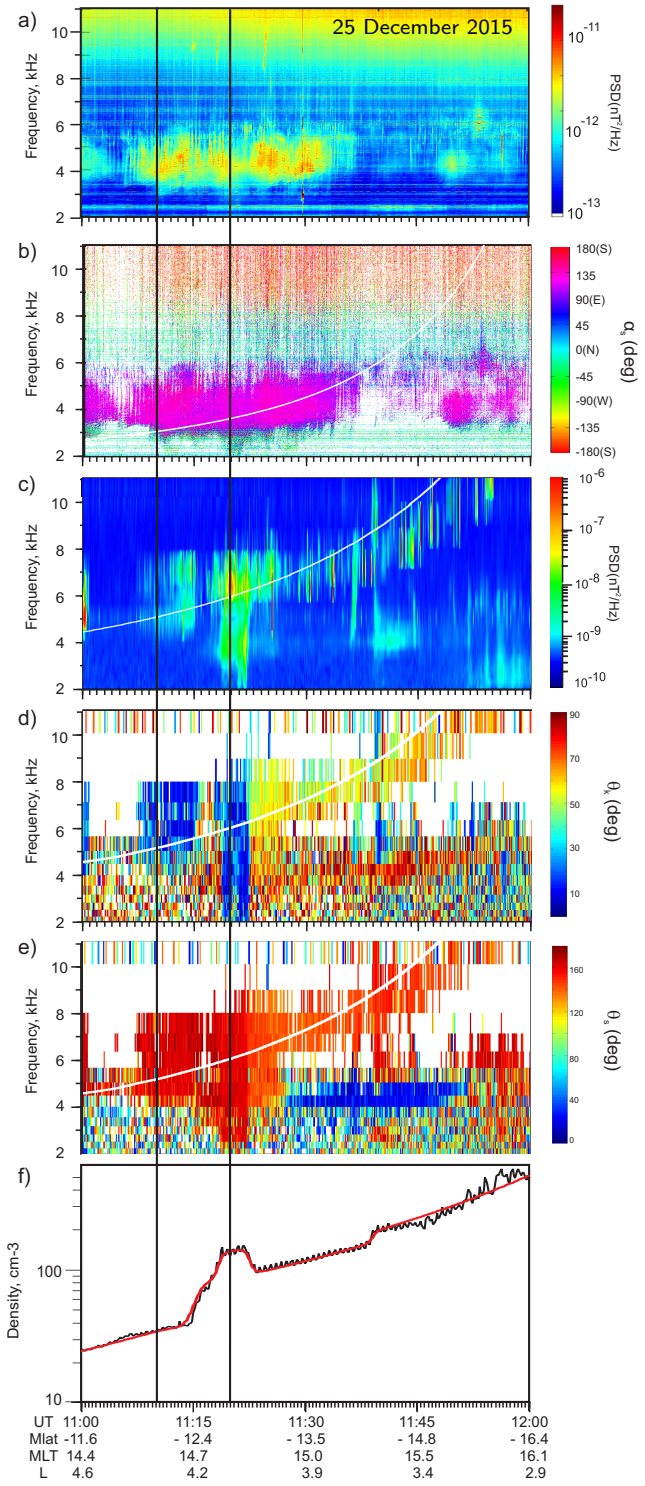

Figure 3. Frequency-time spectrograms of VLF emissions measured at KAN (a), LOZ (b), and by the RBSP-B (c to e) on 25 December 2015 from 11:00 to 12:00 UT. (a) and (c) Magnetic power spectral density; (b) inverse angle of Poynting flux at LOZ; (d) and (e), respecively: polar angles of wave normal and Poynting flux at RBSP-A in the field-aligned coordinate system. White curve shows one half of the equatorial electron gyrofrequency ($f_{ceq}/2$) corresponding to the spacecraft L-shell. Time interval corresponding to the observations of similar signals by KAN and RBSP-A is bounded by gray vertical bars. (f) Electron density derived from EFW data (black) and its smooth fit (red) that is used for ray tracing (Section 4.2).

3.2 VLF emissions observed by RBSP

Overview spectrograms of VLF waves measured by RBSP-B and RBSP-A are shown on panels c) to f) in Figures 2 and 3, respectively. We show RBSP-B first because it spent longer time in the appropriate sector during this event. The waves are seen as multiple amplitude enhancements, some of which are hiss and the other are chorus waves. Electron density determined by EFW measurements is plotted in Figures 2f and 3f. Some enhancements of the wave intensity are clearly correlated with regions of enhanced plasma density. In particular, it is true for a VLF burst observed by RBSP-A from 11:17 to 11:25 UT in the frequency range 3–8 kHz (Figure 3c). Note that the frequency range below 2 kHz is not shown in the plots. It contains rather intense hiss emissions which are not the focus of this paper. At KAN, there was strong interference in this frequency range, and no natural VLF emissions were observed.

The overall frequency-time structure of VLF emissions detected by both RBSP spacecraft is clearly quite different compared to KAN (see Figures 2 and 3). The emission frequency increased from 3–4 to 11 kHz as both spacecraft moved inward. The white and magenta curves on the spectrograms show one half of the equatorial electron gyrofrequency $f_{c\,\mathrm{eq}}$. The frequencies of the VLF emissions observed by RBSP remained near $f_{c\,\mathrm{eq}}/2$ during the entire interval. All waves have almost circular right-hand polarization, i.e., belong to the whistler mode.

Figures 2d and 3c show the wave normal angles with respect to the geomagnetic field. It is seen that VLF signals propagate in the quasiparallel mode with the wave normal angles $\theta_k < 20^\circ$ in a time interval between 11:50 and 12:15 UT for RBSP-B and from 11:08 to 11:23 UT for RBSP-A (in the latter case, the spacecraft observed a localized density enhancement).

Poynting flux of the VLF waves was directed southward, i.e., away from the equator for all observed waves in the case of RBSP-B (Figure 2e) and for most of the waves measured by RBSP-A (Figure 3e). In the case of RBSP-A one sees narrowband emissions with a frequency of about 4 kHz (11:28 to 11:50 UT) and the Poynting flux directed towards the equator which probably are reflected waves originated at higher L-shells, similar to those reported by Parrot et al. (2003).

In spite of the different frequency-time structures of the VLF emissions detected simultaneously by KAN and RBSP, these spectra turn out to be very similar during some fairly short time intervals. These intervals are marked by vertical lines in Figures 2 and 3, and include observations of quasi-periodic emissions. They are discussed in more detail below.

3.3 Conjugate observations of QP emissions by KAN and RBSP-B

Figures 4 and 5 show detailed views of conjugate KAN–RBSP observations for RBSP-A and RBSP-B, respectively.

3.3.1 Correlation with RBSP-A

Figure 4 shows frequency-time spectrograms of VLF emissions obtained at KAN (Figure 4a) and by RBSP-A (Figures 4b and 4c for magnetic and electric components respectively) during the interval from 11:09 to 11:30 UT. At that time the spacecraft crossed a localized plasma density enhancement of 30–40% (Figure 3f). A correspondence of the QP elements on the ground and onboard the spacecraft can be seen in the time interval 11:10 to 11:20 UT. The intensity of VLF waves observed by RBSP-A at that time varied between 10^{-9} and 10^{-8} $\mathrm{nT}^2/\mathrm{Hz}$. We calculated the correlation coefficient R between the spectral power of VLF waves observed at KAN and onboard RBSP-A for the frequency channels 3983, 5019 and 5629 Hz. The interval 11:15 to 11:17 UT was excluded from the correlation search because there was a pause in the VLF emissions measured by RBSP-A. A better correspondence of the QP elements at RBSP-A with those at KAN was observed for the electric field at 5019 Hz and 5629 Hz in time intervals 11:10 to 11:13 UT and 11:17 to 11:20 UT; the correlation coefficients for these intervals are shown in Figures 4d and 4e. The maximum correlation coefficient is about 0.6, and a clear modulation with the periods near 25 s and 35 s is seen in the dependence of R on the time lag for intervals 11:10–11:13 and 11:17–11:20 UT, respectively. These periods match the QP emission quasi-periods during the corresponding intervals.

3.3.2 Correlation with RBSP-B

One-to-one correspondence of the QP elements at the satellite and on the ground is observed from 12:00 to 12:04 UT in the frequency range 3–7 kHz, when the RBSP-

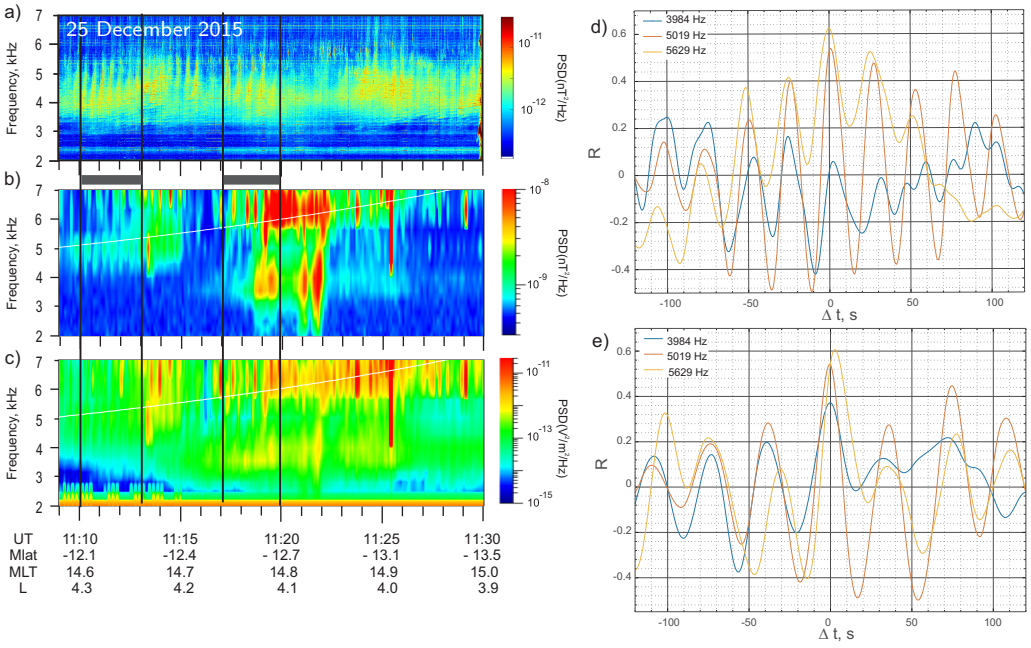

Figure 4. Comparison of VLF emissions observed at KAN and RBSP-A in the time interval 11:09 to 11:30 UT. (a) and (b) Magnetic power spectral density of VLF emissions detected at KAN and by RBSP-A, respectively; (c) electric power spectral density at RBSP-A; (d) and (e) correlation coefficients between the spectral powers of VLF waves measured by RBSP-A and KAN at certain frequencies in time intervals 11:10–11:13 and 11:17–11:20 UT, respectively.

B was at $L \approx 4.5$. At that time RBSP-B moved in the region with a rather smoothly varying cold plasma density (Figure 2f). The QP elements are shown in Figures 5a and 5b. The maximum intensity of waves observed by the spacecraft is below 10^{-9} nT^2/Hz. Figure 5c displays the correlation coefficient R between the magnetic field power of VLF waves observed on the ground and onboard RBSP-B during the time interval shown in Figures 5a and 5b in the frequency range from 4.5 to 6 kHz. The maximum correlation coefficient is only about 0.5, in spite of a clear correspondence between all nine wave bursts at KAN and RBSP-B. This is due to (i) a low cadence of EMFISIS survey mode which is only 4 times shorter than the period of the observed bursts (25 s) and (ii) a fairly weak signal measured by the spacecraft. There is clear modulation in the dependence of R on the time lag between the two envelopes, and the modulation period coincides with the period of QP emissions, which confirms correlation between these signals.

Unfortunately, during this time interval the RBSP-B satellite detected VLF emissions only in the survey mode with a time resolution of 6 s, which does not allow us to reveal a fine structure of the QP elements in the magnetosphere and compare it with KAN observations (Figure 5a).

4 Discussion

In order to verify whether the spacecraft were near the source region of these emissions we compare the obtained wave spectra with the results of calculation of the cyclotron instability growth rate and analyze the possibility of exit of the VLF QP emissions to the ground in the magnetic flux tubes where the spacecraft-ground correlation was observed by RBSP-A and RBSP-B.

4.1 Growth rate of whistler-mode waves

Local growth rates of whistler mode waves were calculated by using the electron pitch angle distribution and plasma parameters measured by RBSP spacecraft. The growth rate was calculated by using the formulas of (Kennel & Petschek, 1966) with a transition from the particle distribution function to differential fluxes, as proposed by Cornilleau-Wehrlin et al. (1985). The calculations were performed for the waves propagating parallel to the geomagnetic field. This is consistent with the low wave normal angles of QP emissions detected by RBSP satellites for the analyzed event (see Figures 2d and 3d).

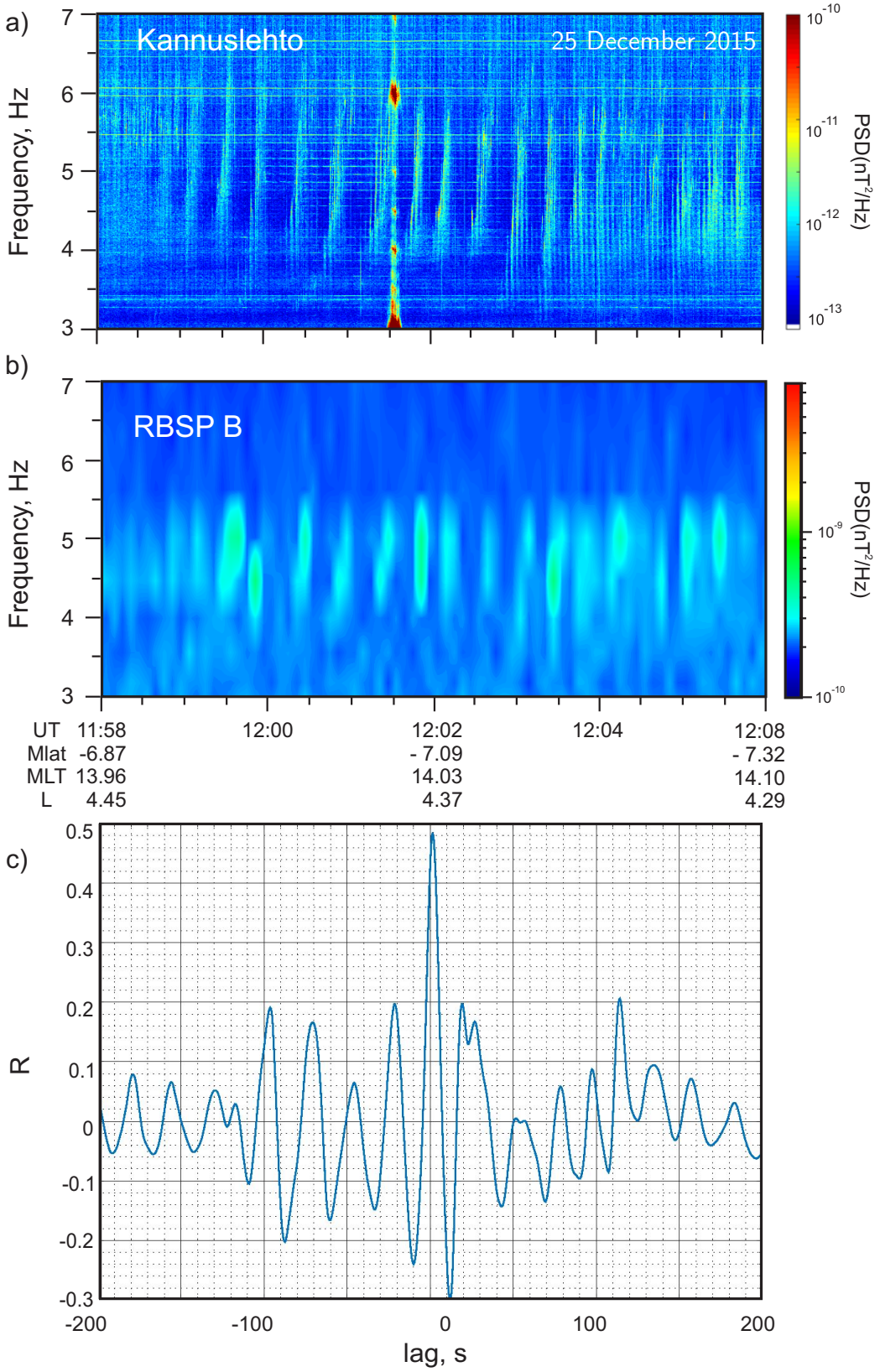

Figure 5. Comparison of VLF emissions observed at KAN and by RBSP-B in the time interval 12:00 to 12:04 UT. (a) and (b) Magnetic power spectral density of VLF emissions detected at KAN and by RBSP-B, respectively. (c) Correlation coefficient between the powers of VLF waves measured by RBSP-B and KAN in the frequency range 4.5 to 6 kHz.

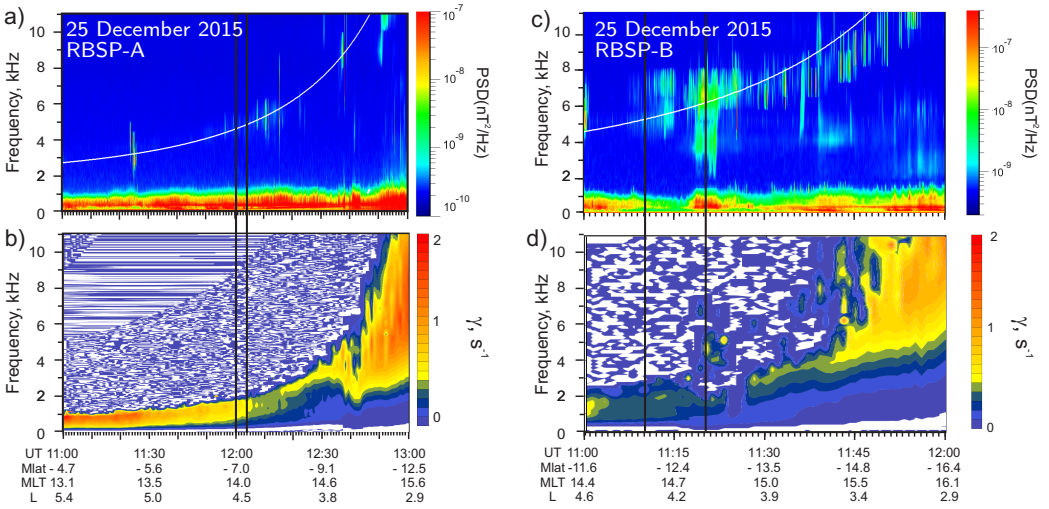

Figure 6. (a) and (c) Magnetic power spectral density of VLF waves; (b) and (d) growth rate of parallel propagating whistler mode waves calculated by using electron distribution functions from HOPE and MAGEIS instruments. Left and right columns show the results for RBSP-B and RBSP-A, respectively.

For these calculations, we averaged the HOPE and MagEIS flux data over one-minute intervals in order to smooth the fluctuations. More details of the procedure are given in (Lyubchich et al., 2017). Electron density profiles along the spacecraft trajectories are shown in Figures 2f and 3f for RBSP-B and RBSP-A, respectively.

The results of growth rate calculations for RBSP-B are shown in Figure 6a. It is seen that at high $L \approx 5$ the growth rate is positive at low frequencies < 1 kHz. As the satellite moves to the lower L shells, the frequency range of positive growth rate extends due to the rapid increasing of its upper frequency related to the increasing electron gyrofrequency. From a comparison of Figures 6a and 6c, it can be seen that the frequency range of the positive growth rate is close to the range of VLF waves detected by RBSP-B only in the beginning of the event (till 11:30 UT). At that time, the waves were observed at frequencies below 1 kHz and did not reveal any quasi-periodic variation. Later, the VLF wave spectra observed by the RBSP-B and the frequency range of the positive growth rate differ significantly. During the observation of QP emissions correlated with KAN at about 12 UT at frequencies of 3–6 kHz, the growth rate is negative in this frequency range.

The results of growth rate calculations for RBSP-A data are shown in Figure 6b. A general frequency increase in the growth rate spectrum is related to the spacecraft inward motion. A localized increase in the growth rate value at frequencies 4 to 6 kHz is evident at 11:17 to 11:25 UT. During that time, the growth rate band matched well the band of the observed QP emissions. Note that it corresponded to the spacecraft crossing of a density enhancement (Figure 3f). After 11:37 UT, the growth rate again increased in value even more significantly, but at higher frequencies. The emissions observed by RBSP-A at that time were not of QP type, and they were not detected at KAN.

4.2 Ray-tracing calculations

The waves generated in the equatorial region can be detected on the ground if they reach the ionosphere, with a low wave normal angle with respect to the vertical direction (Helliwell, 1965; Kuzichev & Shklyar, 2010). We studied the propagation of QP emissions from the equatorial region with the use of the cold-plasma density distribution measured by the RBSP satellites.

Properties of VLF wave propagation and, in particular, the possibility of their observation at the ground, are mainly determined by the cold-plasma density distribution, especially, by different kinds of inhomogeneities, and by the initial wave parameters. As we discussed above, the QP emissions observed by RBSP-A and B satellites correlated with ground based measurements in the region with a smooth change in the cold plasma density for RBSP-B (Figure 2f) and in vicinity of a duct with enhanced density ($d \approx$ 700 km, $\Delta N_e/N_e \approx 45\%$) for RBSP-A (Figure 3f). In both cases the scale of the inhomogeneity is much greater than the characteristic wave length in the considered frequency range. This enables us to use the ray-tracing method for wave propagation modeling.

For the ray-tracing simulations we have used smooth analytical distributions of the plasma density N_e fitted to the measured values. These N_e profiles plotted as solid blue and red curves in Figures 2f and 3f were used in our simulations to define the model dependence of $N_e(L)$. The gyrotropic model was used to get the density distribution along the geomagnetic field ($N_e = N_{e\,\mathrm{eq}}\ (f_c/f_{c\,\mathrm{eq}})$, where the subscript "eq" refers to the values in the equatorial plane). The geomagnetic field was considered in a dipole approximation throughout the simulations.

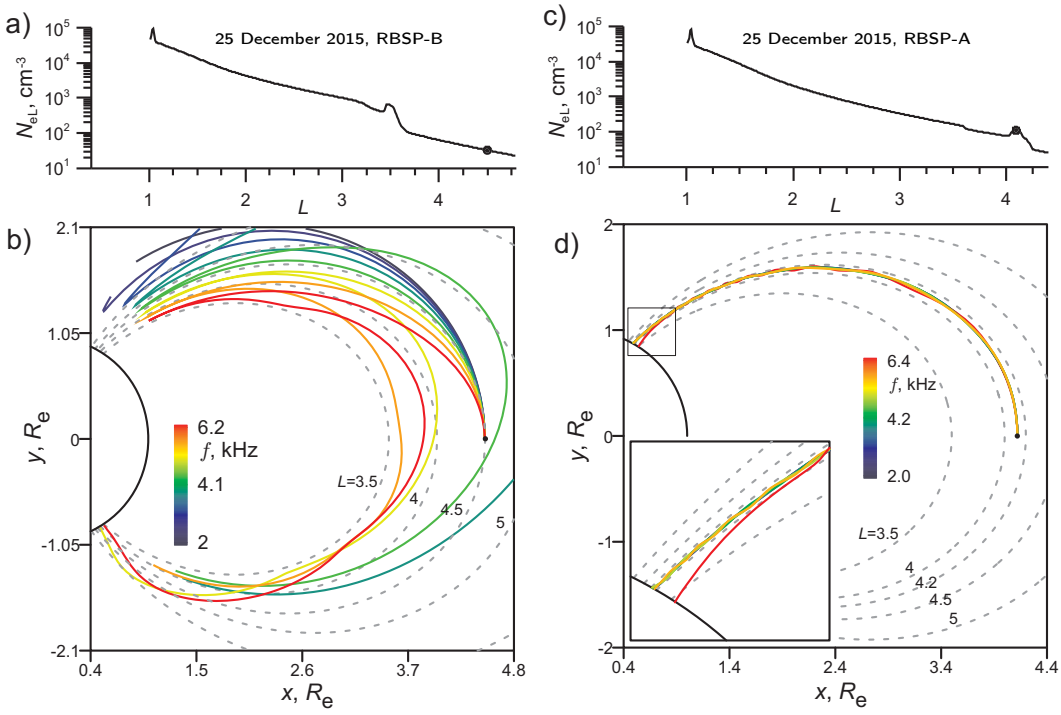

Figure 7. (a) and (c) Model electron density profiles used in ray tracing (see also time dependences in Figures 2f and 3f). (b) and (d) Ray trajectories of VLF waves launched with zero wave normal angle at the geomagnetic equator. The points of launch are shown by dots on the density plots. Line color encodes the frequency. Left and right columns show the results for RBSP-B and RBSP-A, respectively. Dashed gray lines show geomagnetic field lines for the L shells indicated at the lines.

As was mentioned above, the frequency of VLF waves observed by the spacecraft was changing proportional to the local equatorial gyrofrequency (see Figures 2c and 3c). This indicates that the probable source of such waves is related to the development of the cyclotron instability (Trakhtengerts, 1963; Kennel & Petschek, 1966). This is also supported by the measurements of the wave-normal angle which was in the range of about 20° at the measurement point (see Figures 2d and 3d). Thus, the starting points of rays were chosen in the equatorial plane and the initial wave vector was directed along the geomagnetic field ($\theta_k = 0°$). Due to this fact we can consider propagation of waves in the meridional plane only.

4.2.1 Ray tracing from the RBSP-B location

Let us consider the propagation of waves from the point at $L = 4.5$ which corresponds to the RBSP-B location during simultaneous observations with KAN in the frequency band 4–6 kHz (Figure 2). In this region RBSP-B observed a gradual decrease of the plasma density with increasing distance from the Earth without noticeable irregularities (see Figure 2f). The ray tracing results for waves in frequency range 2–6 kHz starting at the equator at $L = 4.5$ with the wave vectors directed along the geomagnetic field are shown in Figure 7b. It is seen that in the considered frequency range all waves are reflected near the point at which their frequency becomes equal to the local value of the lower-hybrid resonance (LHR) frequency (Shklyar & Jiříček, 2000), and most of the waves do not reach the ionosphere. Only higher frequency waves with $f \geq 5$ kHz (which is greater than $f_{c\,\mathrm{eq}}/2 \approx 4.8$ kHz) propagate to the conjugate ionosphere after LHR reflection, but the wave normal angles of these waves at the ionospheric level are very high. Therefore, they wereunable to pass through the ionosphere. Thus, our calculations demonstrate that the waves starting from $L = 4.5$ at the RBSP-B trajectory could not propagate to the ground, in spite of the fact that the QP emissions observed by RBSP-B and KAN were clearly correlated.

4.2.2 Ray tracing from the RBSP-A location

Unlike the RBSP-B case, spectral similarity between the emissions observed by RBSP-A and KAN in the lower frequency band (3–6 kHz) occurred in the region with the cold plasma density duct (Figure 3e). The results of ray-tracing simulations for this case are shown in Figure 7d. The starting point was chosen at the equator at $L = 4.1$ (i.e., inside the density duct). In this case the waves at frequencies below $f_{c\,\mathrm{eq}}/2$ ($f_{c\,\mathrm{eq}} \approx 12.8\ kHz$ for $L = 4.1$) are trapped in the duct. However, trapping of waves with frequencies close to the $f_{c\,\mathrm{eq}}/2$ ($f > 6$ kHz) is violated as they approach the ionosphere (see the expanded view of ray trajectories in the inset in Figure 7d) and afterwards the wave-normal angle rapidly increases during non-ducted propagation. Thus, one should expect that only lower frequency waves which have low wave-normal angles would propagate through the ionosphere and could be detected by a ground station. This is consistent with KAN observations, where only waves below 6 kHz were detected (see Figures 2a and 3a).

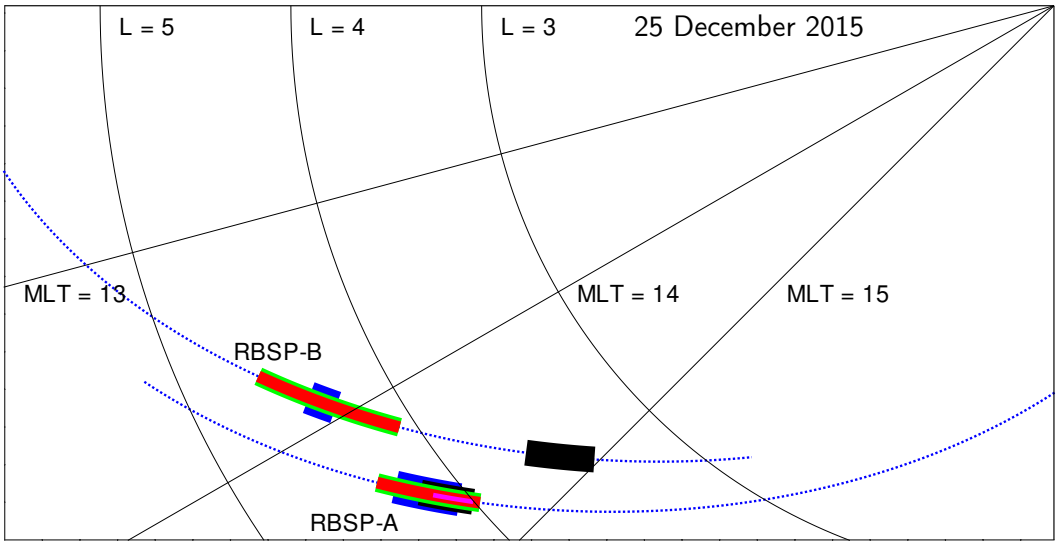

Figure 8. Equatorial projection of spacecraft trajectories during the event of 25 December 2015. Blue dashed lines show the trajectory parts during the time interval of QP observation at KAN. Solid blue, green, red, and magenta segments indicate the time intervals corresponding, respectively, to conjugate QP observations, low wave-normal angles, Poynting vector direction from the equator, and matching between the calculated growth rate and observed wave bands. Black segments indicate crossing of the localized density enhancement. Thin lines show fixed L and MLT values: $L = 3$, 4, and 5, and MLT = 13, 14, and 15 h.

4.3 Possible location of the source of QP emissions

Very close similarity of QP emissions observed simultaneously by KAN and the RBSP spacecraft suggests a common source of these emissions. During both correlation intervals described above, the spacecraft observed the QP emissions at close L shells ($L =$ 4.5 for RBSP-B and $L = 4.4$ to 4.1 for RBSP-A). However, these regions were separated rather far in longitude: the distance between them in geographical longitude was $\Delta\lambda \approx 25^\circ$ (see Figure 1), and the MLT difference was about 0.7 h. The equatorial projection of spacecraft trajectories is shown in Figure 8.

The wave normal angles of the observed emissions were low in both cases of one-to-one correlation. The Poynting flux was directed away from the equator, which would be consistent with the source location in both regions. However, other data support the source location in only one of them.

Indeed, KAN and LOZ angles of arrival (Figures 2b and 3b) indicate the wave propagation in the north-west direction. This agrees well with the wave exit to the ground from the flux tube crossed by RBSP-A from 11:15 to 11:30 UT. On the other hand, this direction does not match the geomagnetic projection of RBSP-B at 12:00 to 12:04 UT that was south-west from KAN.

The same conclusion can be drawn from calculations of whistler mode growth rate: the band of positive growth rate corresponded well to the observed emission band along the RBSP-A trajectory from 11:15 to 11:25 UT, but did not correspond to the QP emissions detected by RBSP-B from 12:00 to 12:04 UT.

Moreover, the possibility of wave propagation in the ducted regime and their exit to the ground is confirmed for observations at RBSP-A but not RBSP-B (cf. Figures 7b and 7d). Recall that QP emissions onboard RBSP-B were correlated with those observed by KAN in the region with a rather smooth change in the cold plasma density, whereas the correlation between KAN and RBSP-A was observed when the spacecraft was in the vicinity of a region (duct) with enhanced plasma density.

To summarize, we think that the entire data set supports the location of possible source region of the considered QP emissions in or very close to the flux tube crossed by RBSP-A from 11:15 to 11:30 UT. Based on KAN and LOZ angles of arrival, which practically did not change during the considered time interval, the source region remained stable with respect to the ground stations during the entire observation interval from 11:10 to 12:40 UT. This stability can be explained by association of this possible source region with a plasma density duct, that could corotate with the Earth and thus remain stable with respect to KAN and LOZ. Indeed, the geomagnetic activity was low, with Kp $\sim$ 2.0 and Dst ~ -4 nT, and the electric field measured by EFW onboard the RBSP-A and RBSP-B (not shown here for brevity) was almost equal to the corotation field, which confirms our assumption.

An enhancement of plasma density was also recorded by RBSP-B at 12:38 to 12:43 UT (Figure 2f). The projection of this enhancement shown in Figure 8 matches well the MLT sector at which the duct was detected by RBSP-A more than one hour before. Therefore, the observed plasma structure remained fairly stable even after the end of the QP event. The question how the waves propagated from their probable generation region (which, as we think, was crossed by RBSP-A at around 11:15 to 11:25 UT) to the re-

gion of their detection by RBSP-B remains open. Note that the propagation took place in both radial and azimuthal directions. A related and also unresolved question is why the waves stopped being detected by RBSP-B at 12:04 UT while they continued being observed at KAN till 12:30 UT. Both magnetospheric refraction and propagation in the Earth-ionosphere waveguide with subsequent wave leakage to the ionosphere should be considered, taking into account much lower wave amplitude measured by RBSP-B outside the probable generation region.

Our results directly confirm, for this specific event, the importance of wave guiding for generation of QP emissions, since their source was found in a duct with enhanced plasma density. Previous studies (e.g., Němec et al., 2018) demonstrated that statistically but indirectly by revealing that the QP events almost always had upper frequencies below one half of equatorial gyrofrequency of electrons. Another indirect confirmation of this fact comes from calculations of one-hop gain of whistler mode waves, that turns out to be about 1 or less, i.e., multiple passes through the amplification region are necessary for wave generation (Lyubchich et al., 2017).

5 Conclusions

We have analyzed a case where quasi-periodic VLF emissions were observed on the ground (KAN station in Finland and LOZ station at Kola Peninsula) and by RBSP spacecraft. Specific feature of this event was that the ground station observed the emissions during a long time interval (10:20 to 12:30 UT), while the RBSP-A and RBSP-B spacecraft observed them during different short time intervals (11:10 to 11:20 and 12:00 to 12:04 UT, respectively). We have revealed a plausible position of the source region of these QP emissions by analyzing all available data and calculating the growth rate and ray trajectories of whistler-mode waves. This probable source region was crossed by only one spacecraft (RBSP-A), and it was related to a localized density enhancement (duct) with a scale of 700 km across the geomagnetic field. The duct could remain stable due to low geomagnetic activity and almost ideal co-rotation of cold plasma. The other spacecraft detected the QP emissions outside the probable source region (at a distance by 0.4 in L and 0.7 h in MLT), and with much lower power. These results directly confirm the importance of guided propagation for the generation of QP emissions and demonstrate transverse spreading of VLF waves in radial and azimuthal directions from a localized source flux tube.

Acknowledgments

Comparison of spacecraft and ground-based data and modeling (A.D., L.T., D.P., A.L., and A.N.) was supported by the Russian Science Foundation (project No. 15–12–20005). The work on the ground-based data was supported by the Academy of Finland under grant No. 315716. The work of O.S. was supported by MSMT CR through the LTAUSA17070 project and by the Praemium Academiae Award from The Czech Academy of Sciences. The authors would like to thank the designers of Van Allen Probes and developers of the instruments (EMFISIS — Craig Kletzing, EFW — John Wygant, HOPE — Herb Funsten, MagEIS — Bern Blake) for the open access to the data. Processing and analysis of the [HOPE, MagEIS, REPT, or ECT] data was supported by Energetic Particle, Composition, and Thermal Plasma (RBSP-ECT) investigation funded under NASA's Prime contract no. NAS5-01072. Van Allen Probe data used in this paper can be found in the EMFISIS (`http://emfisis.physics.uiowa.edu/data/index`), EFW (`http://www.space.umn.edu/rbspefw-data/`), and RBSP-ECT (`http://www.RBSP-ect.lanl.gov/`) archives. KAN data are available at `http://www.sgo.fi/pub_vlf/`. LOZ data are available at `http://pgia.ru/opendata/`.

References

Blake, J. B., Carranza, P. A., Claudepierre, S. G., Clemmons, J. H., Crain, W. R., Dotan, Y., ... Zakrzewski, M. P. (2013). The Magnetic Electron Ion Spectrometer (MagEIS) Instruments Aboard the Radiation Belt Storm Probes (RBSP) Spacecraft. *Space Sci. Rev.*, *179*(1), 383–421. doi: 10.1007/s11214-013-9991-8

Bortnik, J., Thorne, R. M., Li, W., Angelopoulos, V., Cully, C., Bonnell, J., ... Roux, A. (2009). An observation linking the origin of plasmaspheric hiss to discrete chorus emissions. *Science*, *324*(5928), 775-778. doi: 10.1126/science.1171273

Chum, J., & Santolík, O. (2003). Propagation of whistler-mode chorus to low altitudes: divergent ray trajectories and ground accessibility. *Ann. Geophys.*, *23*(12), 3727-3738. doi: 10.5194/angeo-23-3727-2005

Cornilleau-Wehrlin, N., Solomon, J., Korth, A., & Kremser, G. (1985). Experimental study of the relationship between energetic electrons and ELF waves observed on board GEOS: A support to quasi-linear theory. *J. Geophys. Res.*, *90*(A5),

4141–4154. doi: 10.1029/JA090iA05p04141

Demekhov, A. G., Manninen, J., Santolík, O., & Titova, E. E. (2017). Conjugate ground–spacecraft observations of VLF chorus elements. *Geophys. Res. Lett.*, *44*(23), 11735-11744. doi: 10.1002/2017GL076139

Engebretson, M. J., Posch, J. L., Halford, A. J., Shelburne, G. A., Smith, A. J., Spasojevic, M., ... Arnoldy, R. L. (2004). Latitudinal and seasonal variations of quasiperiodic and periodic VLF emissions in the outer magnetosphere. *J. Geophys. Res.*, *109*(A05). doi: 10.1029/2003JA010335

Fedorenko, Y., Tereshchenko, E., Pilgaev, S., Grigoryev, V., & Blagoveshchenskaya, N. (2014). Polarization of ELF waves generated during "beat-wave" heating experiment near cutoff frequency of the Earth-ionosphere waveguide. *Radio Science*, *49*(12), 1254-1264. doi: 10.1002/2013RS005336

Funsten, H. O., Skoug, R. M., Guthrie, A. A., MacDonald, E. A., Baldonado, J. R., Harper, R. W., ... Chen, J. (2013). Helium, Oxygen, Proton, and Electron (HOPE) mass spectrometer for the Radiation Belt Storm Probes mission. *Space Sci. Rev.*, *179*(1), 423–484. doi: 10.1007/s11214-013-9968-7

Helliwell, R. A. (1965). *Whistlers and related ionospheric phenomena.* Palo Alto, Calif.: Stanford Univ. Press.

Inan, U. S., & Bell, T. F. (1977). The plasmapause as a vlf wave guide. *J. Geophys. Res.*, *82*, 2819-2827.

Kennel, C. F., & Petschek, H. E. (1966). Limit on stably trapped particle fluxes. *J. Geophys. Res.*, *71*(1), 1–28. doi: 10.1029/JZ071i001p00001

Kletzing, C. A., Kurth, W. S., Acuna, M., MacDowall, R. J., Torbert, R. B., Averkamp, T., ... Tyler, J. (2013). The Electric and Magnetic Field Instrument Suite and Integrated Science (EMFISIS) on RBSP. *Space Sci. Rev.*, *179*(1), 127–181. doi: 10.1007/s11214-013-9993-6

Kurth, W. S., De Pascuale, S., Faden, J. B., Kletzing, C. A., Hospodarsky, G. B., Thaller, S., & Wygant, J. R. (2015). Electron densities inferred from plasma wave spectra obtained by the Waves instrument on Van Allen Probes. *J. Geophys. Res. Space Phys.*, *120*, 904-914. doi: 10.1002/2014JA020857

Kuzichev, I. V., & Shklyar, D. R. (2010). On full-wave solution for VLF waves in the near-Earth space. *J. Atmos. Sol.-Terr. Phys.*, *72*(13), 1044–1056. doi: 10.1016/j.jastp.2010.06.008

Li, W., Ma, Q., Thorne, R. M., Bortnik, J., Kletzing, C. A., Kurth, W. S., ... Nishimura, Y. (2015). Statistical properties of plasmaspheric hiss derived from Van Allen Probes data and their effects on radiation belt electron dynamics. *jgra*, *120*(5), 3393-3405. doi: 10.1002/2015JA021048

Lyubchich, A. A., Demekhov, A. G., Titova, E. E., & Yahnin, A. G. (2017). Amplitude–frequency characteristics of ion–cyclotron and whistler-mode waves from Van Allen Probes data. *Geomagn. Aeron.*, *57*(1), 40–50. doi: 10.1134/S001679321701008X

Manninen, J. (2005). *Some aspects of ELF-VLF emissions in geophysical research* (Doctoral dissertation, Sodankylä Geophysical Observatory Publications, No. 98, `http://www.sgo.fi/Publications/SGO/thesis/ManninenJyrki.pdf`). Retrieved from `http://www.sgo.fi/Publications/SGO/thesis/ManninenJyrki.pdf`

Manninen, J., Demekhov, A. G., Titova, E. E., Kozlovsky, A. E., & Pasmanik, D. L. (2014). Quasiperiodic VLF emissions with short-period modulation and their relationship to whistlers: A case study. *J. Geophys. Res.*, *119*(A6), 3544-3557. doi: 10.1002/2013JA019743

Martinez-Calderon, C., Katoh, Y., Manninen, J., Kasahara, Y., Matsuda, S., Kumamoto, A., ... Miyoshi, Y. (2019). Conjugate observations of dayside and nightside VLF chorus and QP emissions between Arase (ERG) and Kannuslehto, Finland. *Journal of Geophysical Research: Space Physics*, *124*. doi: 10.1029/2019JA026663

Martinez-Calderon, C., Shiokawa, K., Miyoshi, Y., Keika, K., Ozaki, M., Schofield, I., ... Kurth, W. S. (2016). ELF/VLF wave propagation at subauroral latitudes: Conjugate observation between the ground and Van Allen Probes A. *J. Geophys. Res. Space Phys.*, *121*(A6). doi: 10.1002/2015JA022264

Němec, F., Bezděková, B., Manninen, J., Parrot, M., Santolík, O., Hayosh, M., & Turunen, T. (2016). Conjugate observations of a remarkable quasiperiodic event by the low-altitude DEMETER spacecraft and ground-based instruments. *J. Geophys. Res. Space Phys.*, *121*, 8790-8803. doi: 10.1002/2016JA022968

Němec, F., Hospodarsky, G. B., Bezděková, B., Demekhov, A. G., Pasmanik, D. L., Santolík, O., ... Hartley, D. (2018). Quasiperiodic whistler mode emissions

observed by the Van Allen Probes spacecraft. *J. Geophys. Res. Space Phys.*, *123*, 8969-8982. doi: 10.1029/2018JA026058

Němec, F., Santolík, O., Pickett, J. S., Parrot, M., & Cornilleau-Wehrlin, N. (2013). Quasiperiodic emissions observed by the Cluster spacecraft and their association with ULF magnetic pulsations. *J. Geophys. Res. Space Phys.*, *118*, 4210-4220. doi: 10.1002/jgra.50406

Parrot, M., Santolík, O., Cornilleau-Wehrlin, N., Maksimovic, M., & Harvey, C. (2003). Magnetospherically reflected chorus waves revealed by ray tracing with CLUSTER data. *Ann. Geophys.*, *21*, 1111-1120.

Santolík, O., Chum, J., Parrot, M., Gurnett, D. A., Pickett, J. S., & Cornilleau-Wehrlin, N. (2006). Propagation of whistler mode chorus to low altitudes: Spacecraft observations of structured ELF hiss. *J. Geophys. Res.*, *111*(A10). doi: 10.1029/2005JA011462

Santolik, O., & Gurnett, D. A. (2002). Propagation of auroral hiss at high altitudes. *Geophys. Res. Lett.*, *29*(10), 1191–1194.

Santolík, O., & Gurnett, D. A. (2003). Transverse dimensions of chorus in the source region. *Geophys. Res. Lett.*, *30*(2). doi: 10.1029/2002GL016178

Santolík, O., Kletzing, C. A., Kurth, W. S., Hospodarsky, G. B., & Bounds, S. R. (2014). Fine structure of large-amplitude chorus wave packets. *Geophys. Res. Lett.*, *41*, 293-299. doi: 10.1002/2013GL058889

Santolík, O., Parrot, M., & Lefeuvre, F. (2003). Singular value decomposition methods for wave propagation analysis. *Radio Sci.*, *38*(1), 1010. doi: 10.1029/2002JA009791

Santolík, O., Pickett, J. S., Gurnett, D. A., Menietti, J. D., Tsurutani, B. T., & Verkhoglyadova, O. (2010). Survey of Poynting flux of whistler mode chorus in the outer zone. *J. Geophys. Res.*, *115*(A7). doi: 10.1029/2009JA014925

Sazhin, S. S., & Hayakawa, M. (1994). Periodic and quasiperiodic VLF emissions. *J. Atmos. Terr. Phys.*, *56*, 735-753.

Semenova, V. I., & Trakhtengerts, V. Y. (1980). On specific features of the LF waveguide propagation. *Geomagn. Aeron.*, *20*(6), 1021-1027.

Shklyar, D., & Jiříček, F. (2000). Simulation of nonducted whistler spectrograms observed aboard the MAGION 4 and 5 satellites. *J. Atmos. Sol.-Terr. Phys.*, *62*(5), 347–370.

Titova, E. E., Demekhov, A. G., Manninen, J., Pasmanik, D. L., & Larchenko, A. V. (2017). Localization of the sources of narrow-band noise VLF emissions in the range 4–10 kHz from simultaneous ground-based and Van Allen Probes satellite observations. *Geomagn. Aeron.*, *57*(6), 706-718.

Titova, E. E., Kozelov, B. V., Demekhov, A. G., Manninen, J., Santolık, O., Kletzing, C. A., & Reeves, G. (2015). Identification of the source of quasiperiodic VLF emissions using ground-based and Van Allen Probes satellite observations. *Geophys. Res. Lett.*, *42*(15), 6137-6145. doi: 10.1002/2015GL064911

Trakhtengerts, V. Y. (1963). The mechanism of generation of very low frequency electromagnetic radiation in the Earth's outer radiation belt. *Geomagn. Aeron.*, *3*(3), 365.

Wygant, J. R., Bonnell, J. W., Goetz, K., Ergun, R. E., Mozer, F. S., Bale, S. D., ... Tao, J. B. (2013). The electric field and waves instruments on the Radiation Belt Storm Probes (RBSP) mission. *Space Sci. Rev.*, *179*(1), 183-220. doi: 10.1007/s11214-013-0013-7